IN VITRO SIMULATION OF TORQUE-INDUCED ROTATOR CUFF DAMAGE

BY

JOHN FRANCIS SHANLEY IV

THESIS

Submitted in partial fulfillment of the requirements
for the degree of Master of Science in Mechanical Engineering
in the Graduate College of the
University of Illinois at Urbana-Champaign, 2018

Urbana, Illinois

Adviser:

Assistant Professor Mariana E. Kersh

Abstract

Various aspects of rotator cuff tears have been studied in depth, including the primary pathogenesis and mechanical properties. There is, however, a lack of information available on the injury mechanics associated with sudden torque loading of the shoulder. To investigate the mechanical response of the Supraspinatus tendon and the joint capsule when exposed to repeated near-instantaneous torques, an in vitro test apparatus was developed. Supraspinatus and capsular reaction forces, capsular surface strains, and shoulder accelerations were measured over 30 cycles of applied torque. A decreasing logarithmic decay was found in the difference between the initial and final loads within each cycle. A generalized force-displacement fiber recruitment model was used to determine the protective role of the capsule by evaluating changes in stiffness. The results suggest that while relatively more damage happens in the first few high-torque load cycles, sudden adduction loading injuries are likely fatigue-based in nature.

Acknowledgements

I would like to express my thanks and gratitude to Professor Mariana Kersh for providing the opportunity for me to work on this project, and for her time and tireless support in helping me complete this thesis. I would also like to extend a special thanks to Tissue Biomechanics Lab members Hafizur Rahman, Woojae Kim, Hyunggwi Song, and James Nie for their assistance and contributions during testing. And finally, thank you to my friends, family, parents, and Rachel for supporting me through it all.

Contents

1 Literature Review

1.1 Anatomy of the Shoulder and Rotator Cuff

The shoulder is an upper extremity joint connecting the arm to the torso. The shoulder joint is the intersection of the scapula, clavicle, and humerus, and is surrounded by numerous muscles including the rotator cuff (Supraspinatus, Subscapularis, Infraspinatus, and Teres Minor), as well as other muscles (Deltoid, Pectoralis major, Teres major, Biceps, Triceps, Coracobrachialis, and Latissimus dorsi) [1, 35]. The rotator cuff is a system of four muscle-tendon units that originate on the scapula and insert into the proximal humerus [33] (Figure 1). The purpose of the rotator cuff is to stabilize the shoulder by constraining the position of the proximal humerus and aiding larger skeletal muscles in creating humeral motion. For example, in arm abduction the Supraspinatus has been shown to have larger force contributions at lower arm angles (0° to 45°) than it does at higher arm angles [19]. Teres Minor, Infraspinatus, and Subscapularis all contribute to humeral rotation and horizontal flexion/extension [30].

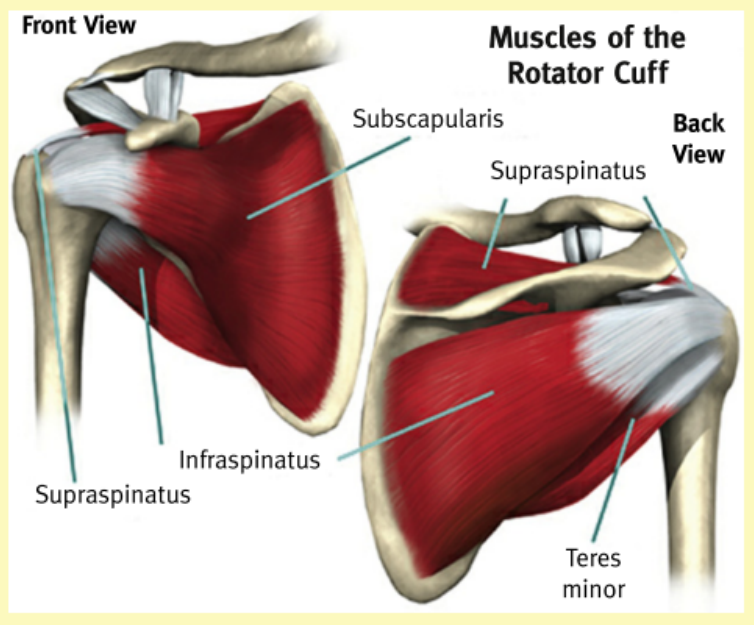

Figure 1: Diagram of rotator cuff muscles and tendons: Supraspinatus, Infraspinatus, Subscapularis, and Teres Minor [2].

There are four muscle-tendon units that make up the rotator cuff: the Supraspinatus (superior), Infraspinatus (posterior), Subscapularis (anterior), and Teres Minor (posterior, inferior) (Figure 2). All four of these muscles originate on the scapula and insert into the head of the humerus [33]. The middle deltoid (which originates on the acromion and inserts into the deltoid tuberosity on the humerus) is a key contributor to abduction [40]. This is important because this study is focused on ab/adduction

motion of shoulder.

1.2 Physiology of the Rotator Cuff

It has been shown that while there are several muscles that are active in elevating (abducting) the arm [30], the middle deltoid and Supraspinatus muscles are the primary shoulder abductors [19]. One study looked at relative muscle contributions to humeral abduction by measuring the force in the deltoid as certain combinations of muscles were used [30]. This study was done to simulate the effect of rotator cuff tearing and find the relationship between rotator cuff muscles and the deltoid during arm abduction. The results are summarized in the table shown in Figure 3. Moment arm information as a function of abduction angle has been collected in multiple studies [1, 40] and is best summarized in Figure 4. The combination of relative force information and moment arms can be used in force balance equations to scale loading conditions, as the relationship between increasing the load carried in the hand during abduction and force required for abduction has been shown to be approximately linear (Järvholm et al. [16] in Figure 5).

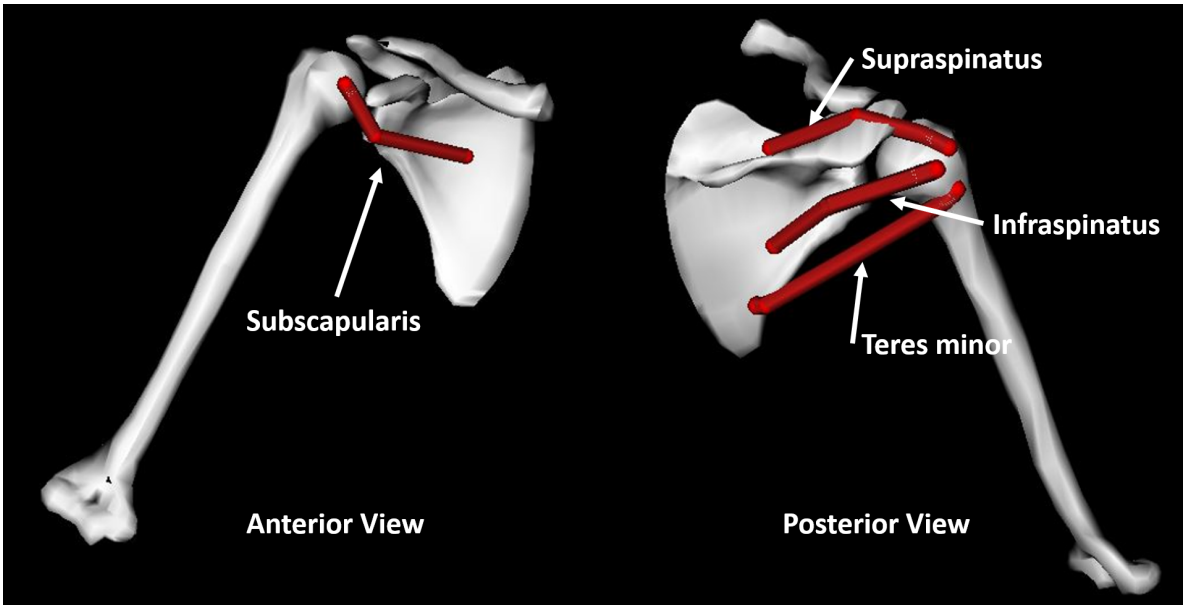

Figure 2: Geometry of Rotator Cuff muscles, shown with centered anchor points.

Active muscles	30°	60°	90°	120°
Deltoid and entire rotator cuff	20 ± 21[a]	82 ± 48[a]	168 ± 51[a]	198 ± 56
Deltoid, infraspinatus-teres minor, and subscapularis	32 ± 12[a]	122 ± 53[a,b]	184 ± 52[a]	172 ± 34
Deltoid and supraspinatus	24 ± 21[a]	153 ± 58[b,c]	200 ± 61[a]	194 ± 46
Deltoid only	100 ± 30[c]	208 ± 40[c]	280 ± 24[c]	210 ± 20

Values are given as the mean ± SD (n = 5).
For each angle, data with the same superscripts are not significantly different (overall significance level of 5%).

Figure 3: Deltoid force [N] required to abduct shoulder with different rotator cuff tearing contributions [30]. This information was important in developing our Supraspinatus load estimates.

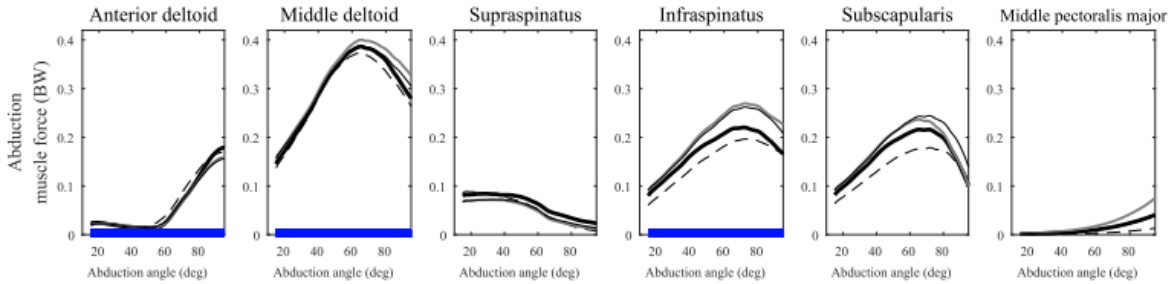

Figure 4: Diagram of muscle moment arms for pure abduction of the shoulder [40].

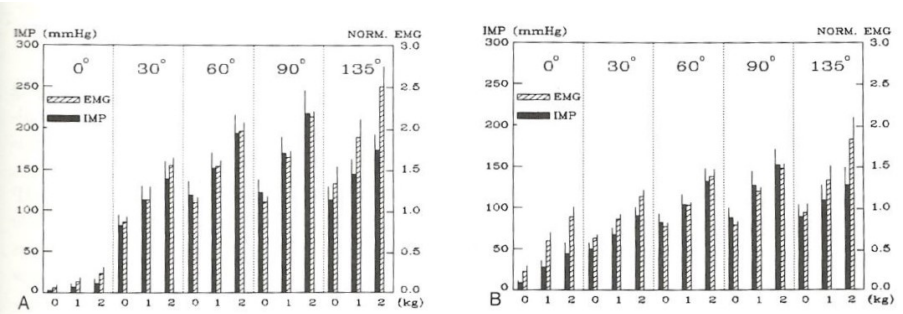

FIGS. 4A AND 4B. Mean IMP and normalized EMG in the supraspinatus muscle at five different abduction angles with (A) a straight elbow and (B) a flexed elbow. In each position the hand was loaded with 0, 1, or 2 kg. Vertical lines extending above the bars indicate the SEMs.

Figure 5: Linear relationship between intramuscular pressure and weight held in the hand during abduction from EMG study [16].

1.3 Clinical Problem

Rotator cuff tears are the most common cause of pain, weakness, and disability in the shoulder, appearing in over 20% of the population and increasing in prevalence with age [4, 22, 28]. Adding further complication to the general study of rotator cuff injury is the prevalence of asymptomatic tears to the rotator cuff. This is when an individual has at least a partial tear of the rotator cuff but does not have symptoms or pain and is consequently unaware of the injury. One study conducting shoulder exams

found that of the 664 subjects, 147 had rotator cuff tears–65.3% of which were asymptomatic [28]. Studies looking at such tears suggest that roughly half of patients with asymptomatic tears will develop symptoms within 3 years of the injury [41]. This often makes determining the cause of such tears difficult, as they may be inappropriately attributed to events occurring closer to the onset of symptoms.

Independent of failure mode, many previous studies have reported that the vast majority of rotator cuff tears are to the Supraspinatus tendon, usually around approximately 1cm away from the humeral insertion [22, 28]. Of these tears, it has been observed in one study that approximately 85% are centered in the anterior portion of the tendon [36]. Interestingly, the anterior portion of the tendon has been shown to have a higher failure stress (16.5 $\pm$ 7.1MPa) than the middle (6.0 $\pm$ 2.6MPa) and posterior (4.1 $\pm$ 1.3MPa) portions of the tendon [14]. Cadaveric studies of rotator cuff tearing report that between 23% and 30% of cadavers are found to have some degree of rotator cuff tearing [28].

1.4 Risk Factors

There is some disagreement over what the primary pathogenesis of rotator cuff tearing is [2]. Some argue that the leading cause of rotator cuff tearing is caused by degeneration over time due to a variety of factors including poor blood supply or collagen deterioration among other factors [12, 24]. Studies looking at rotator cuff tears [33] have identified several risk factors, including genetics, smoking, hypercholesterolemia, and occupational hazards. These factors are all contributors to enhance the age-related deterioration that can lead to injury or disease of the rotator cuff.

Others argue that the leading cause is subacromial impingement of the Supraspinatus, resulting in wear of the tissue and leading to rotator cuff tears [20]. Subacromial Impingement Syndrome is caused by the acromion pinching down on the avascular region of the Supraspinatus and biceps tendons. It is commonly found in athletes, and while it does increase in prevalence with time, young athletes are also at risk for subacromial impingement [13, 37].

1.5 Who Has Studied Rotator Cuff Tears?

There have been many studies on the various elements of rotator cuff tears, which take a look at the family of injuries in a multitude of ways. It is well established that shoulder pain is linked to occupational hazards, including heavy workloads, repetitive motions, and compromising postures [3, 38]. Research has looked at factors ranging from the geometric properties of the Supraspinatus tendon [17], to strain distributions during tensile rupture tests of the Supraspinatus tendon [21]. The implications certain activities (like pitching in baseball) have on tearing the rotator cuff have also been studied

[10, 29]. Additionally, tears to the Supraspinatus tendon decrease the stability of the shoulder and show significant decreases in the elastic modulus of the Infraspinatus and Subscapularis [27]. While there are many studies investigating possible causes and effects of rotator cuff tears, there is a noticeable void in the literature when it comes to the injury mechanism involved in sudden adduction loading.

Nearly all of the studies currently presented in literature that look at traumatic events believed to cause tearing in one or more rotator cuff muscles are centered around over-hand throwing motions, like those seen in professional sports (e.g. a baseball pitcher) [25, 29]. There is little published work pertaining to rotator cuff tears injured through other motion profiles, such as abduction and adduction rotation of the shoulder. According to Dr. Rick Goding, these injuries occur in industries where manual labor is used. Inspiration for the methods used in this study were searched for in literature, however the lack of published work on recreating tears in cadavers by mimicking real-world trauma scenarios limited the external influence on the direction of this project.

1.6 Why Study Rotator Cuff Tears?

Rotator cuff tears and resulting surgeries are on the rise in the United States, with a reported 141% increase in surgical procedures between 1996 and 2006 [6]. An estimated 272,000 rotator cuff repairs were performed in the United States in 2006 [15], and with the estimated average cost for a surgical repair cycle around $5,900 [23], there is an increasing need to find better repair and injury prevention methods. There is also evidence suggesting that rotator cuff tear prevalence increases with age, particularly in people older than 60 [34]. With the average age of the US population increasing [26] (Figure 6), rotator cuff tears will increase as well.

Rotator cuff tears (like most physical injuries and conditions) can be treated in a variety of ways, often including surgical options. While many people prefer non-surgical treatment methods for cost or other reasons, one study has shown long term cost-benefits of choosing a surgical route for rotator cuff tears. This is particularly true for younger patients: the average lifetime savings of 30-39 year olds opting for surgery over alternative treatments is $77,662 [18]. These findings help motivate research that better enables and prepares surgeons for procedures to correct rotator cuff injury, with an interest in creating a better and more informed surgical environment.

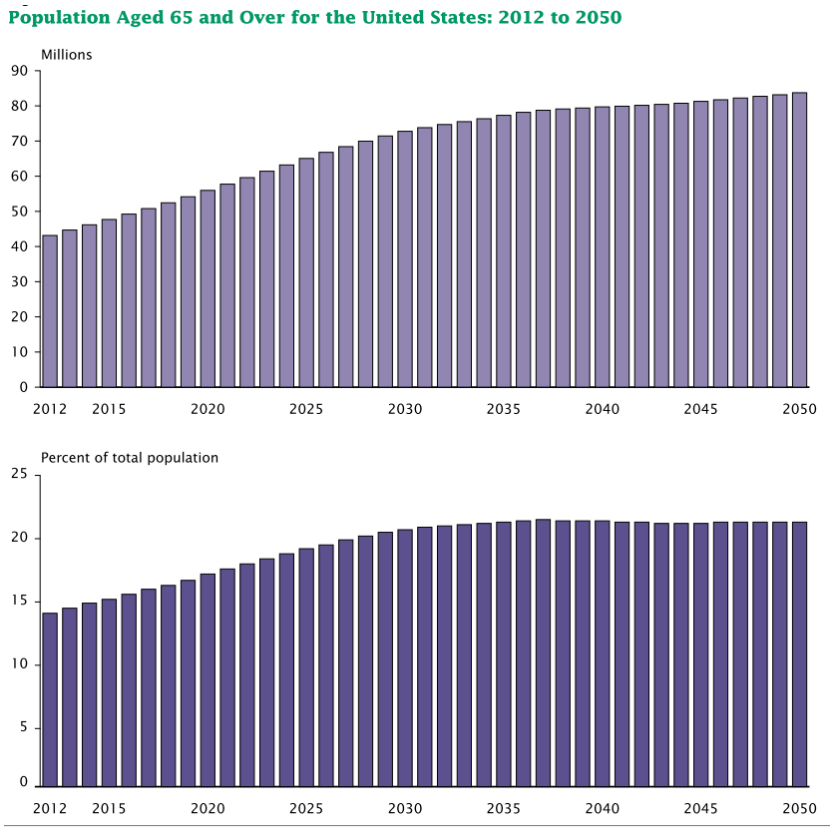

Figure 6: Increasing age of population in the United States [26].

Aside from tendon degeneration and subacromial impingement, there is a third potential primary factor that leads to tearing of the rotator cuff: injury due to sudden or fatigue related stresses placed on the shoulder. In some industries where high-power hand-operated equipment is used (e.g. construction), the soft tissues in the shoulder can be subjected to sudden large loads that have the potential to lead to injury. The mechanisms behind damage due to sudden torque loading that originate from drill use have not previously been studied.

1.7 Drilling Position

The position in which an operator holds a drill has a direct impact on the relative risk of injury during drill use. Documentation from drill manufacturers (like the Makita XFD07Z user manual [7]) offer vague guidelines for best practices, suggesting that drills should be operated from balanced positions and that operators should not overreach. In a study investigating the relative muscle forces for operating a drill in a range of over-head drilling positions, Anton et al. [3] showed that drilling closer to the body (less extreme arm/shoulder position) minimized shoulder forces. The range of positions and corresponding data from this study are shown in Figures 7 and 8, respectively. These findings are

consistent with the reported mode of injury [Dr. Rick Goding], where drill operators have their arm elevated and away from the body.

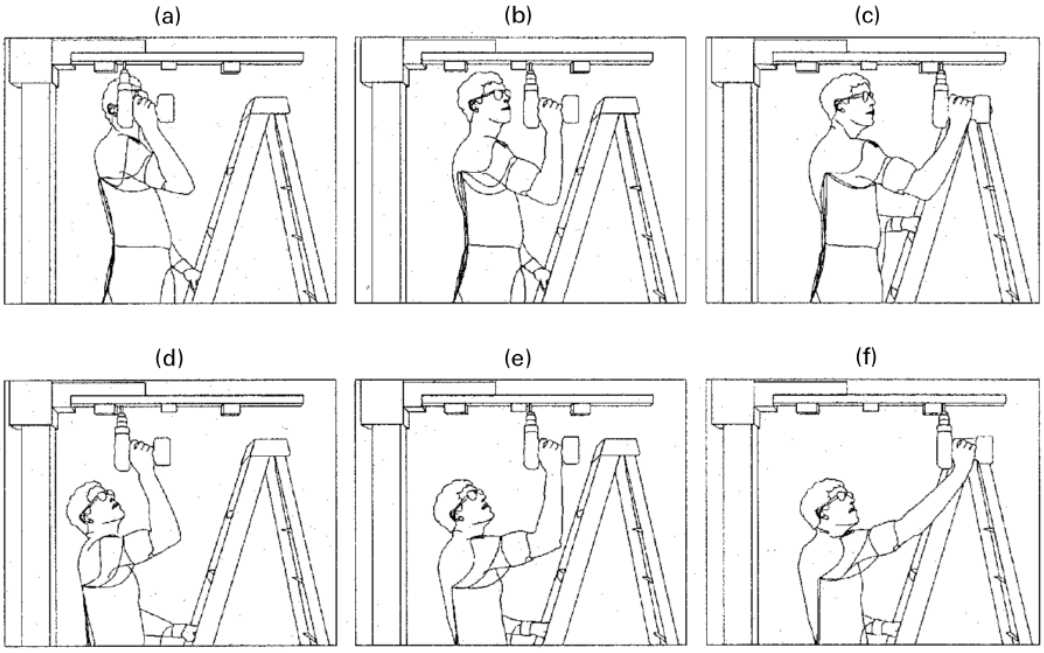

Posture of the overhead drilling task using a close, middle and far reach position while standing on the lower and higher step of a stepladder. (a) Close reach, high step; (b) Middle reach, high step; (c) Far reach, high step; (d) Close reach, low step; (e) Middle reach, low step; (f) Far reach, low step.

Figure 7: Overhead drilling positions studied by Anton et al. [3].

		Close reach		Middle reach		Far reach	
	Step	Mean	SE	Mean	SE	Mean	SE
Anterior deltoid	High	30.18	2.41	53.88	2.98	115.77	3.89
	Low	98.91	3.17	134.73	4.85	153.11	8.14
Biceps brachii	High	379.07	12.61	298.96	30.96	422.31	44.10
	Low	112.98	49.82	272.90	21.91	645.82	65.07
Triceps brachii	High	22.93	2.11	21.55	1.64	28.71	2.11
	Low	102.67	4.41	55.92	3.19	56.64	4.19
Shoulder joint moment	High	7.03	0.42	13.78	0.408	24.18	0.554
	Low	13.07	0.493	20.95	0.583	28.74	0.612

SE = standard error.

Figure 8: EMG [% Normalized] and shoulder moment [Nm] data from varying drilling position [3].

1.8 Tissue Clamping Methods

There are many ways to rigidly fix an object, however many of these can lead to problems during data collection, which make clamp selection an important step in experimental setup. The main reported issues that other experiments have had with clamping soft tissues are slipping of the muscle or tendon

from the clamp, and early rupture of the specimen due to stress concentrations and altered tissue geometry as a result of clamping [32]. To account for these issues, research groups have developed several methods and devices for clamping soft tissues. One of the most popular solutions is the freeze clamp or "cryo jaw", and offshoots of this idea [31]. Figure 9 provides one such design of a freeze clamp. Freeze clamps work by pumping liquid nitrogen or CO_2 through channels in the clamp to rapidly cool the clamp and attached tissue. Typically, they have crinkled clamping faces to increase the surface area that the tissue has in contact with the clamp.

Freeze clamping has been shown to greatly improve the pull-out force of tissues over traditional clamps, but is also expensive and requires a lot of maintenance. Other methods of clamping tissue include self-tightening clamps, sandpaper-based clamps, and clamps with optimized adhering surfaces [32]. Additionally, companies like Instron sell a range of clamp variants based on the type of tissue being tested and the tensile force requirements of the test.

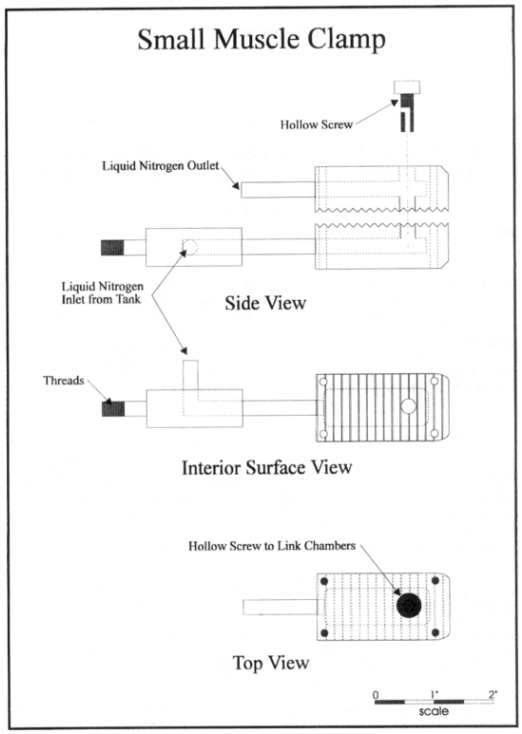

Figure 9: Example freeze clamp design for circulating coolant and rapidly chilling clamped portion of specimen [31].

2 IN VITRO SIMULATION OF TORQUE-INDUCED ROTATOR CUFF DAMAGE

2.1 Introduction

Rotator cuff tears are the most common cause of shoulder pain, appearing in over 20% of the population, and are increasing in prevalence with age [22, 28, 33]. While the rotator cuff is comprised of four separate muscles positioned about the shoulder, the majority of rotator cuff tears are to the Supraspinatus tendon, near the humeral insertion [22, 28]. Of Supraspinatus tears, approximately 85% are centered in the anterior half of the tendon [36]. With an estimated 272,000 rotator cuff repairs performed in the United States in 2006 [15], and an estimated average cost of $5,900 for a typical rotator cuff surgical repair cycle [23], there is a pressing need to better understand the injury mechanism.

The cross-sectional area of the Supraspinatus tendon has been shown to decrease with age [17] and may therefore increase tendon stress due to muscle forces transmitted through the tendon. Few studies, however, have investigated the actual failure mechanism of rotator cuff tears. Itoi et al. measured the tensile and rupture properties of the Supraspinatus in cadavers and found that the ultimate load was significantly greater in the anterior portion of the tendon [14]. Miller et al. measured the strain distribution during cyclic fatigue tensile loading (to failure) and found that over the course of testing the direction of strain shifted from the anterior to posterior portion of the tendon [21]. Neviaser et al. conducted a similar fatigue tensile loading study in rats, and found that subjecting specimens to large strains led to reduced stiffness over the course of testing as a result of fiber rupture. Neviaser suggests that in low strain tests an increase in stiffness can be attributed to the recruitment of fibers and the associated redistribution of loads to undamaged fibers, while high strains may exceed the capacity of these compensatory mechanisms [24]. These findings indicate that initial stages of fatigue may consist of an uncrimping of fibers and a redistribution of loading in the tissue. These studies provide some insight into the mechanics of tendon injury under axial tension, however, there is little information regarding the injury mechanism initiating rotator cuff tears. The exception to this is sports-related injuries, thought to occur during over-hand throwing motions, in which the shear and compressive forces as well as adduction torques are significant [10, 25, 29].

Shoulder pain is linked to occupational hazards, including heavy workloads and repetitive motions [38]. It is also associated with kinematic profiles that include abduction or adduction of the shoulder, most commonly seen in manual labor settings involving drill usage [Dr. Rick Goding]. The position of the shoulder during drill usage has a considerable effect on the muscle load, and is associated with higher stress in the shoulder. Using EMG data, Anton et al. demonstrated that most of the forces in the

shoulder (anterior deltoid, biceps, and total shoulder moment) are lower when holding the drill closer to the body [3]. Anton concluded that operating a drill further from the body has a higher likelihood of injury to the rotator cuff and shoulder complex as a whole. During drill usage, the shoulder is in an abducted position and experiences a rise in torque from the drill about the anterior-posterior axis of the glenohumeral joint center. In some scenarios, for example when a drill hits rebar and stops the drill bit from spinning, an abrupt increase in abduction torque may occur that is then countered by adduction muscle forces and the shoulder capsule aiming to stabilize the arm. The capsule is responsible for creating a stable fulcrum for shoulder motion, and is the primary restraint against translation of the humeral head [5]. The Supraspinatus tendon (along with the other rotator cuff tendons) fuse with the capsule [9], making it important to evaluate both together to determine their combined response to torque loads. Understanding the injury mechanism during drill use will be useful in evaluating techniques for repairing rotator cuff tears.

In the case of both sports and work-related injuries, we hypothesize that an adduction torque applied to the shoulder contributes to rotator cuff injury. An in vitro test apparatus was developed to evaluate the mechanics of the Supraspinatus tendon and superior portion of the shoulder capsule during repeated exposure to an impulse torque load. The test apparatus was designed to pretention the Supraspinatus to a theoretical force required to hold a drill and measure Supraspinatus tension and surface strain of the tendon-capsule complex during sudden shoulder adduction.

2.2 Methods

Test Apparatus

A custom in vitro apparatus was designed to apply a sudden adduction torque to the humerus while the Supraspinatus is under tension. The apparatus (Figure 10) was built from an aluminum frame supporting a drill (Makita; Figure 10-1), which was connected to a mechanical arm (Figure 10-4) via an electromagnetic clutch (Ogura; Figure 10-3). A flywheel (Figure 10-2) was coupled to the drill to compensate for the inertia of the mechanical arm (Figure 10-4). The mechanical arm was constrained such that it could only rotate about the axis of the drill. This arm was connected to a 3D printed fixture holding the distal end of the humerus (Figure 10-5). The scapula was secured in a second 3D printed fixture that was rigidly fixed to the frame. The activation and deactivation of the drill and clutch were automated using a Raspberry Pi microcontroller, relay switches, limit switches, and electronic actuators.

The Supraspinatus muscle (the primary rotator cuff muscle used in humeral abduction [2, 4, 22]) was clamped and tensioned (Figure 10-6) via wire cabling using a high-torque gear motor (TSINY DC

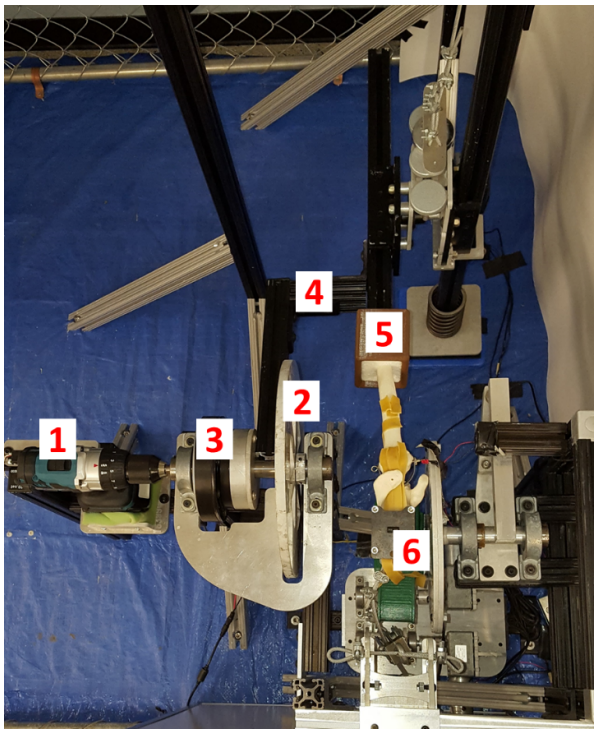

Figure 10: Experimental test apparatus. A power drill (1) and flywheel (2) were coupled via an electromagnetic clutch (3) to a mechanical arm (4). The mechanical arm was connected to the humeral end of a cadaver shoulder (5). The Supraspinatus tendon was clamped (6) to a cable system that used a load cell to measure Supraspinatus tension.

motor). The calculation of tensile loads for Supraspinatus is described in the next section. An S-load cell (Phidgets 500kg) was placed in-line with the Supraspinatus tension cable and used to measure the Supraspinatus tension during testing (sampling frequency = 62.5Hz). Linear acceleration of the mechanical arm was recorded using an accelerometer (Delsys Trigno Wireless EMG System) at 1000Hz.

Supraspinatus Tension

The kinematic pose used to estimate the pretension in the deltoid and Supraspinatus was derived from the posture assumed during drill usage. Specifically, the arm was assumed to be 90° in abduction and bent 90° at the elbow. When an operator is using a drill, we assumed that three primary components contribute to the torque applied to the shoulder: mass of the user's arm ($M_{Forearm}$ and $M_{Humerus}$), mass of the drill (M_{Drill}), and the force resulting from cutting (Cutting Load) (Figure 11).

Assuming a constant cutting load from the drill, the reaction torque τ at the shoulder was calculated as:

$$\tau = g * [d_{Forearm} * \left(M_{Forearm} + \ M_{Drill} + \ \frac{Cutting\ Load}{g} \right) + d_{Humerus} * \ M_{Humerus}] \qquad (1)$$

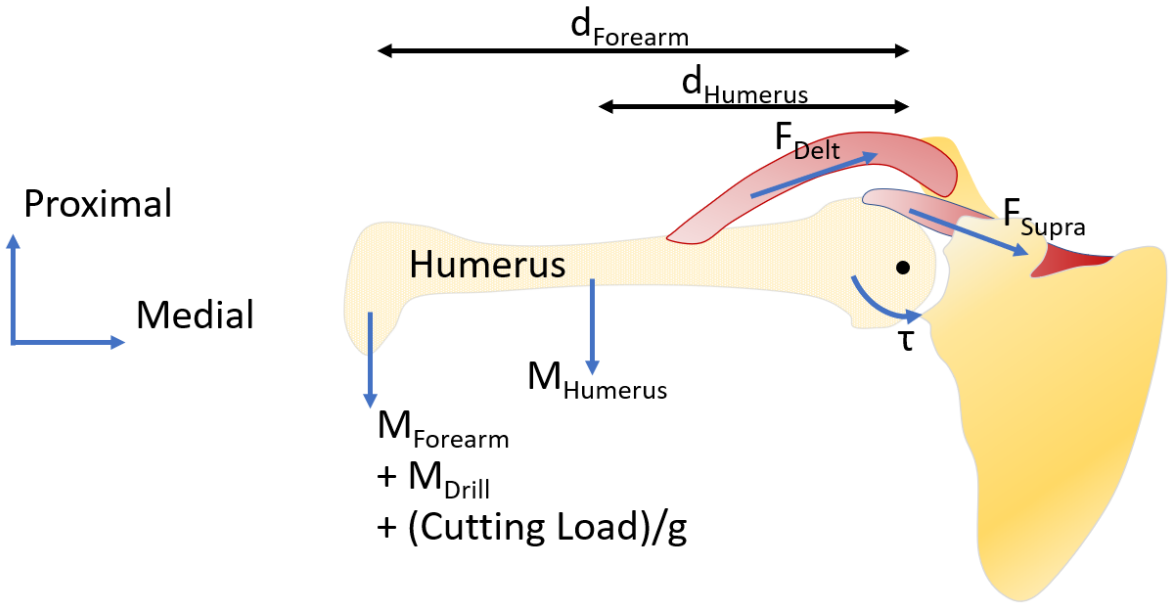

Figure 11: Diagram of external loads ($M_{Forearm}$, M_{Drill}, cutting load, and $M_{Humerus}$) acting on shoulder during drill usage. Internal muscle forces from the deltoid (F_{Delt}) and Supraspinatus (F_{Supra}) also shown.

where g = gravity; $d_{Forearm}$ = the length of the humerus; $d_{Humerus}$ = the length to the center of mass of the humerus, measured from the humeral end (Figure 11).

Anthropometric scaling data [39] was used to estimate the mass of the arm for each specimen as a function of total body mass. Therefore, glenohumeral torque depended only on the height (H) and mass (BM) of the individual, as well as the load from the drill (Equations 2-5).

$$d_{Forearm} = 0.186 * \ H \tag{2}$$

$$d_{Humerus} = 0.436 * \ d_{Forearm} \tag{3}$$

$$M_{Humerus} = 0.028 * \ BM \tag{4}$$

$$M_{Forearm} = 0.022 * \ BM \tag{5}$$

The mass of the drill, 2.7kg, was based on specifications for a Makita 18-Volt LXT Brushless Lithium-Ion 1/2in. Cordless Driver Drill. The cutting load of the drill (i.e. the reaction force from the drill on the operator's hand) was experimentally determined by attaching a block of wood to a rotatable

platform configured to measure torque using a Phidgets 200kg button load cell. Using a 1/4in drill bit in wood, 15 holes were drilled: the average cutting torque of the drill was measured, from which cutting load was calculated to be 6.03 $\pm$ 0.357N.

The two primary muscle contributors to abduction are the Supraspinatus and middle deltoid [19]. At 90° of abduction, the moment arms for Supraspinatus and middle deltoid are approximately 14mm and 28mm, respectively [1]. Assuming that the arm is in a static position, the torque τ is assumed to be balanced by the action of these muscles such that:

$$\tau = (F_{Delt} * 0.028 + F_{Supra} * 0.014) \tag{6}$$

Using data from Sharkey et al. [30], the ratio between Supraspinatus force and middle deltoid force is approximately 0.8. Therefore, the theoretical Supraspinatus force for 90° of abduction was calculated as:

$$F_{Supra} = \frac{\tau}{0.1960} \tag{7}$$

Surface Strain Measurements

Separation of the superior capsule and Supraspinatus tendon was not possible and therefore strain of the tendon-capsule complex was measured. Displacement and strain data was measuring using a 3x4 grid drawn on the surface of the capsule over the Supraspinatus tendon resulting in nine strain regions per specimen. To account for the pre-tensioning of the Supraspinatus, strain was calculated with respect to the displacements at the beginning of each cycle (not the displacements before testing). The grid was aligned with the tensile axis (Figure 12). A camera (Panasonic Lumix FZ200) was used to record the capsular surface grid (100fps) for analysis in MATLAB. The video files were converted to images. The center of each grid point was manually digitized within each image and used to calculate displacements and strains throughout the surface.

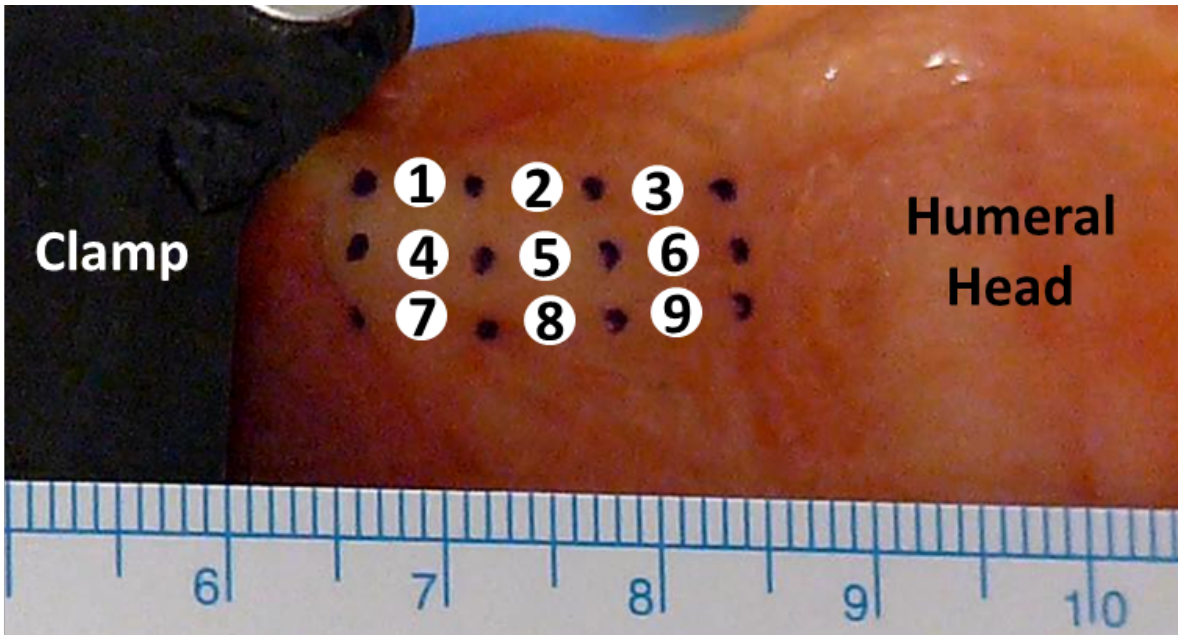

Figure 12: The Supraspinatus tendon was clamped near the aponeurosis of the distal tendon insertion, and a 3x4 dot matrix was drawn over the capsule surface (black dots). The regions between the dots (numbered 1-9) were used in the strain evaluation process.

Specimen Preparation and Testing

Fresh-frozen shoulder cadavers (n = 5) were used for testing. Specimens were thawed at room temperature for 24 hours, then dissected to remove skin, fat, and all soft tissues except for Supraspinatus and the shoulder capsule. The coracoid process and acromion were removed to allow uninhibited access and visibility to Supraspinatus. Next, the distal end of the humerus and distal scapula were potted in two-part epoxy (Smooth-On). The proximal end of the Supraspinatus was severed and placed in a clamp connected to the load cell via wire cabling. The clamp was placed as close to the aponeurosis of the distal tendon insertion as possible to ensure that only the Supraspinatus tendon was held in tension, not the muscle. A series of magnets were used to help secure the humerus in the abducted position.

Each test cycle included three phases of testing. First, the arm was placed at 90° of abduction and the Supraspinatus muscle was tensioned (Figure 13: Phase I). With the specimen secured in the test apparatus and the muscles appropriately tensioned, the drill was activated to full speed, after which the clutch engaged sending a sudden adduction torque to the cadaver and overpowering the magnets used to hold the humerus (Figure 13: increase in force at beginning of Phase II). Once a certain angle of powered adduction was reached (for our tests this angle was 27°), a limit switch was activated which in turn released the clutch and the arm was allowed to settle in its adducted state (Figure 13: Phase II), before being manually raised back up to its original position (Figure 13: transition between Phase II and III). During each test cycle, both the camera and accelerometer were manually started once

the drill was actuated to full speed, and manually deactivated upon the specimen coming to a resting stop. This procedure was repeated for 30 load cycles for each specimen at two-minute intervals. If necessary, specimens were re-tensioned to the phase I target value in between all tests.

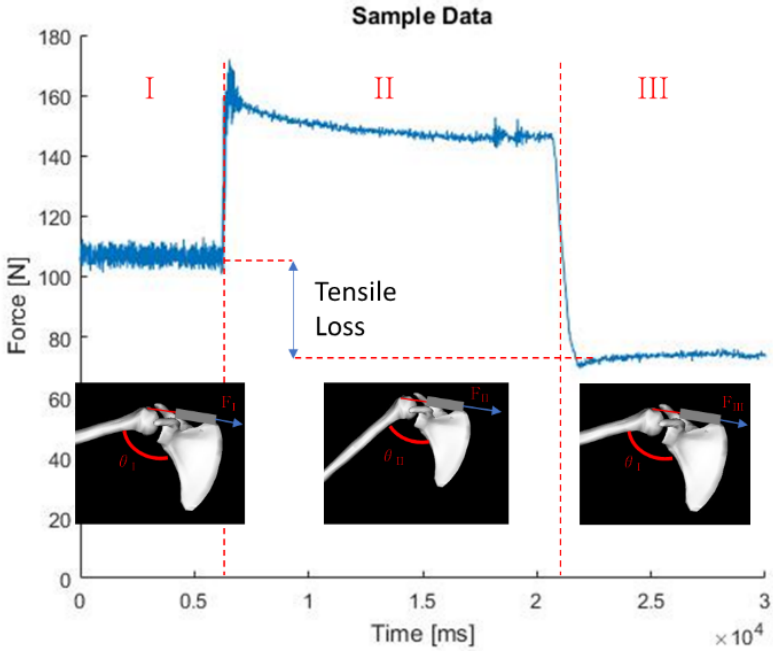

Figure 13: Stages of a test cycle–Specimen is held in tension (I), the clutch engages, the arm adducts and settles (II), and is manually returned to the initial position (III).

Data Analysis

All control software and load cell data acquisition code was written in Python 2.7. Load cell force, accelerations, and strain image data from the camera was processed in MATLAB. Differences in acceleration between initial and final cycles were compared using paired t-tests. Loss in tensile strength was quantified by comparing (unpaired t-test) the initial Supraspinatus tensile force during phase I to the force after the specimen was passively returned to the initial position in phase III. Using the net displacement of the capsule-tendon construct and measured tensile force during powered adduction, we analyzed the force-displacement curves during each cycle. We identified three distinct phases of stiffness during each test: an initial low stiffness (k_1) followed by two sequential increases in stiffness (k_2 and k_3). The three stiffness values were evaluated over time to identify changes in the capsule-tendon construct due to repeated adduction torque. Finally, we evaluated the surface strain measurements to determine whether repeated adduction torque resulted in changes in the superior capsule strain distribution. For all analyses, alpha values for significance was set to 0.05.

2.3 Results

Supraspinatus Tension and Powered Adduction

The average force used to pretension Supraspinatus was 100 ± 10.6N (Table 1). Acceleration data was successfully acquired in four specimens. There was no significant difference in the amount of powered acceleration over the course of testing within a given specimen (Figure 14, p = 0.389). The mean peak acceleration across all specimens was 24.53 ± 1.69m/s^2.

Table 1: Specimen size parameters and theoretical Supraspinatus loads.

Specimen	Age (years)	Height (cm)	Weight (kg)	Supraspinatus Force (N)
S2	60	183	86.2	112
S5	52	170	59.0	88
S6	52	188	77.1	109
S8	57	188	49.9	91
S9	58	183	68.0	100
Mean	55.8	182.4	68.0	100
Std	3.6	7.4	14.3	10.6

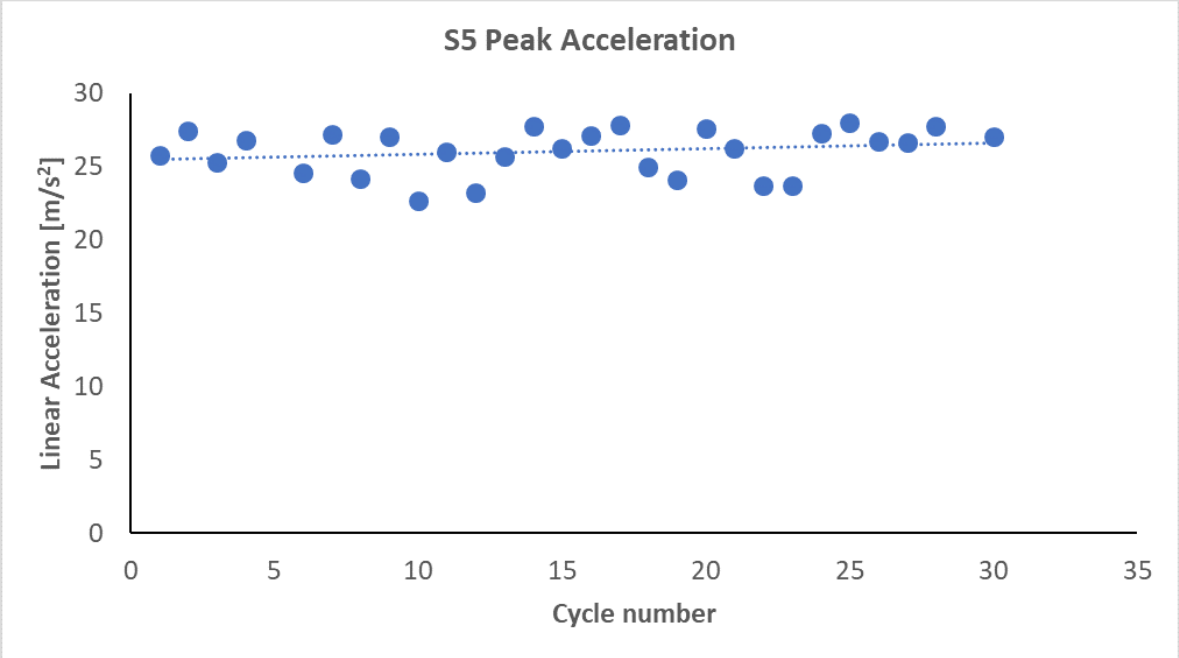

Figure 14: Representative peak acceleration over test cycles. Other specimens showed a similarly flat trajectory over the course of testing.

Tensile Loss

We successfully measured the tensile loss in 76% of all trials in four of the five specimens. Technical difficulties during testing prevented acquisition of data in all test cycles, including a fifth specimen which only yielded 5 data points. Loss in tensile strength was defined as decreases in the static tension at Phase III compared to the initial tension during Phase I (Figure 13). For most specimens, the loss

in tensile strength over the course of testing followed a logarithmic decay (Figure 15) – that is, the greatest loss in tensile strength occurred in the initial cycles.

All specimens experienced an immediate loss in tensile strength after the first cycle (26.1 ± 9.9%). By the 4^{th} cycle, the loss in tensile strength decreased to 12.6 ± 8.1% (p = 0.046) (Figure 15, Table 2). At cycle 7, loss in tensile strength further decreased to 10.7 ± 9.12% (p = 0.047) after which there were no significant changes in the loss of tensile strength between cycle seven and the last cycles during testing (p = 0.187).

Table 2: Percent tensile loss data: mean, standard deviation, number of data points, and p-value for an unpaired t-test comparing the cycle mean to the cycle 1 data. p-values not reported when n < 3.

Cycle	Mean	Std	n	p-value
1	26.1	9.94	5	—
2	25.5	8.66	4	0.920
3	19.4	12.49	4	0.398
4	12.6	8.13	5	0.046
5	16.6	15.48	2	—
6	12.9	9.90	3	0.117
7	10.7	9.12	4	0.047
8	22.7	—	1	—
9	9.3	6.08	3	0.040

Stiffness

Force-displacement data during powered adduction was analyzed for the first seven cycles in four of the five specimens. Three of those four specimens exhibited two or three distinct regions of stiffness: initial stiffening, moderate stiffening, and high stiffening (Figure 16). The remaining specimen did not follow any noticeable trends and was not considered for further analysis.

The overall stiffness decreased by an average of 48.3% in two of the three specimens and increased by 32.7% in one specimen (Table 3). When we analyzed the stiffness in cycles 1-7, the stiffness was highest in region 3 (k_3 = 54.65 ± 17.92), and lowest in region 1 (k_1 = 2.86 ± 10.29). The intermediate stiffness k_2 was 19.30 ± 18.31.

Table 3: Overall stiffness for each specimen over the first 7 cycles.

Stiffness [N/mm]			
Overall	S5	S8	S9
C1	23.51	27.35	37.08
C2	17.97	56.08	30.63
C3	24.83	23.46	36.37
C4	31.41	16.64	42.99
C5	NaN	17.08	43.56
C6	13.04	15.94	53.67
C7	10.41	16.16	49.20

The initial low stiffness region (k_1) decreased at a rate of 2.68N/mm per cycle for S8, while k_2 increased in two specimens and moderately decreased in S8. Overall, for k_2, the stiffness increased at a rate of

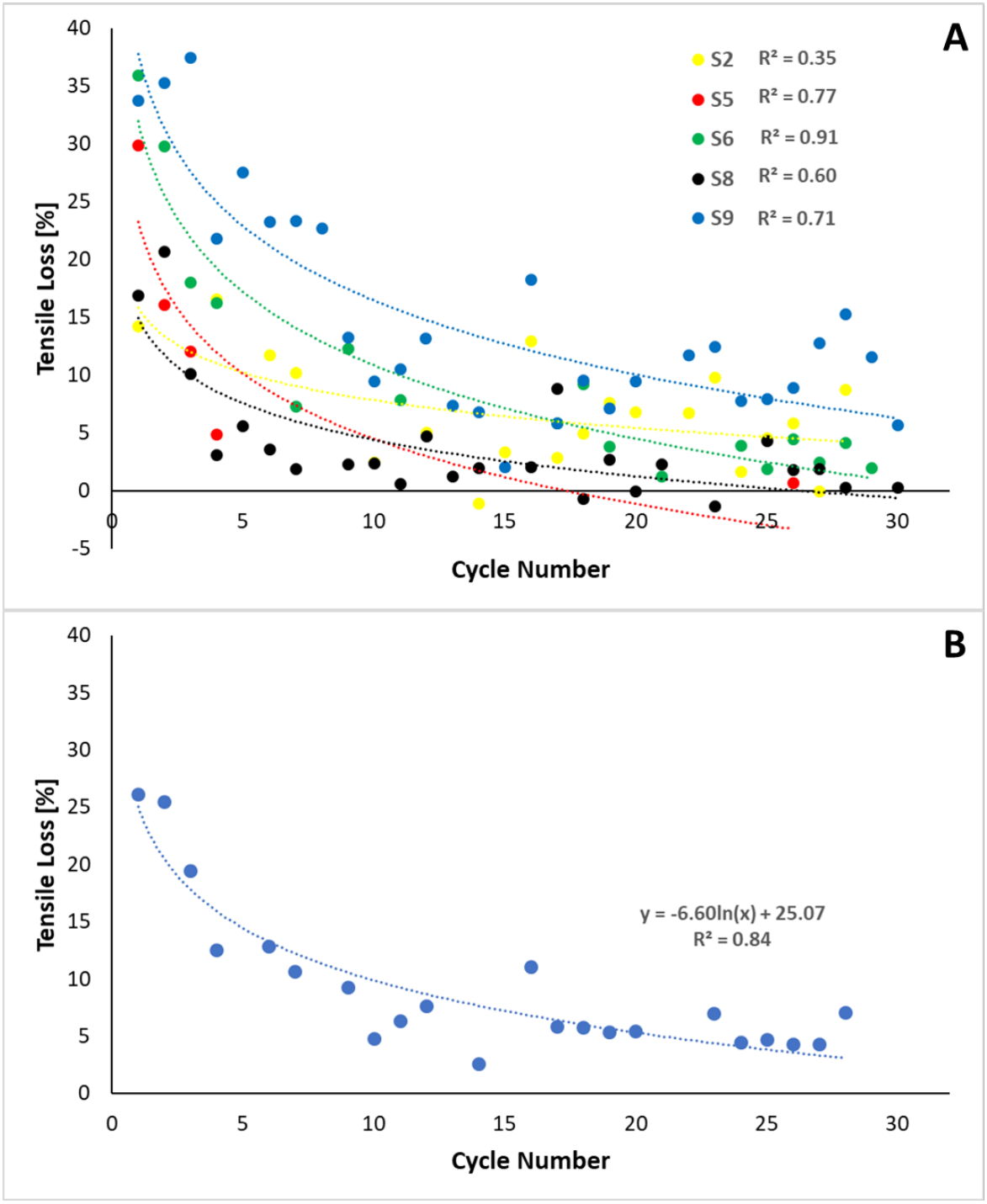

Figure 15: (A) Tension lost in each cycle for all specimens, normalized to each specimen's target (calculated) initial tension. Due to issues during testing, not all specimens have tension loss values for all 30 cycles. (B) Average tensile loss followed a logarithmic trend ($tensile\ loss = -6.60 * ln(cycle) + 25.07$); only specimens with three or more data points were used in (B).

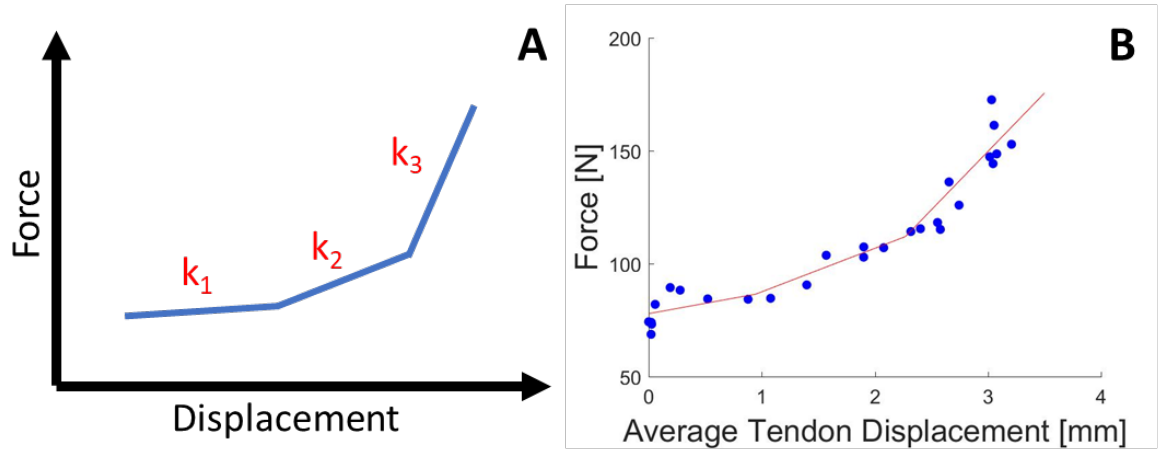

Figure 16: Generalized Force-Displacement damage model (A), shown with the stiffnesses for the evaluated specimens. An example of fitting this model to experimentally collected data is shown (B).

0.71N/mm per cycle. The high stiffness region towards the end of powered adduction, k_3, decreased at a rate of 2.03N/mm per cycle (Figure 17, Table 4).

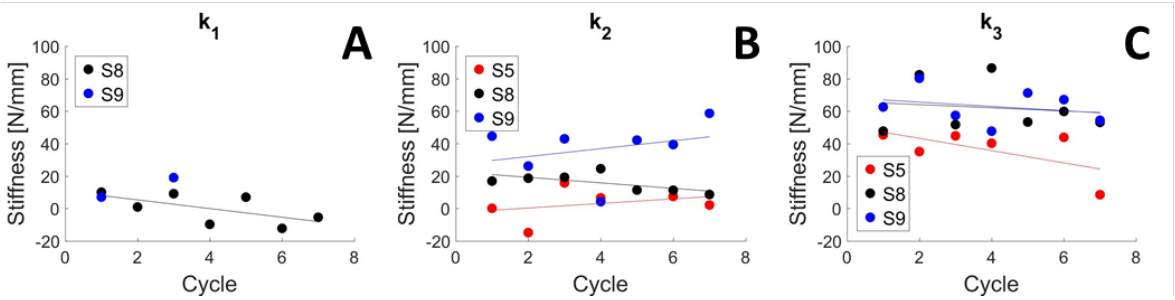

Figure 17: Region 1 (A) shows initial tendon lengthening for healthy tissue. Region 2 (B) shows fully-recruited tendon stiffness. Region 3 (C) shows the gradual decay in stiffness when both the tendon and capsule are being pulled.

Table 4: Regional stiffness data for all specimens. Note: 'NaN' is a placeholder for unavailable data points. Specimens S5 and S9 showed either little or no initial tendon lengthening (k_1).

	Stiffness [N/mm]								
	k_1			k_2			k_3		
	S5	**S8**	**S9**	**S5**	**S8**	**S9**	**S5**	**S8**	**S9**
C1	NaN	10.06	7.02	0.13	16.90	44.58	45.40	47.67	62.58
C2	NaN	0.91	NaN	14.85	18.67	26.16	35.10	82.42	80.27
C3	NaN	9.13	19.03	15.80	19.26	42.94	44.78	51.71	57.35
C4	NaN	-9.74	NaN	6.60	24.51	4.21	40.23	86.56	47.65
C5	NaN	7.00	NaN	NaN	11.38	42.15	NaN	53.31	71.19
C6	NaN	12.25	NaN	7.44	11.25	39.41	43.88	59.82	67.11
C7	NaN	-5.42	NaN	2.15	8.64	58.68	8.51	53.08	54.36

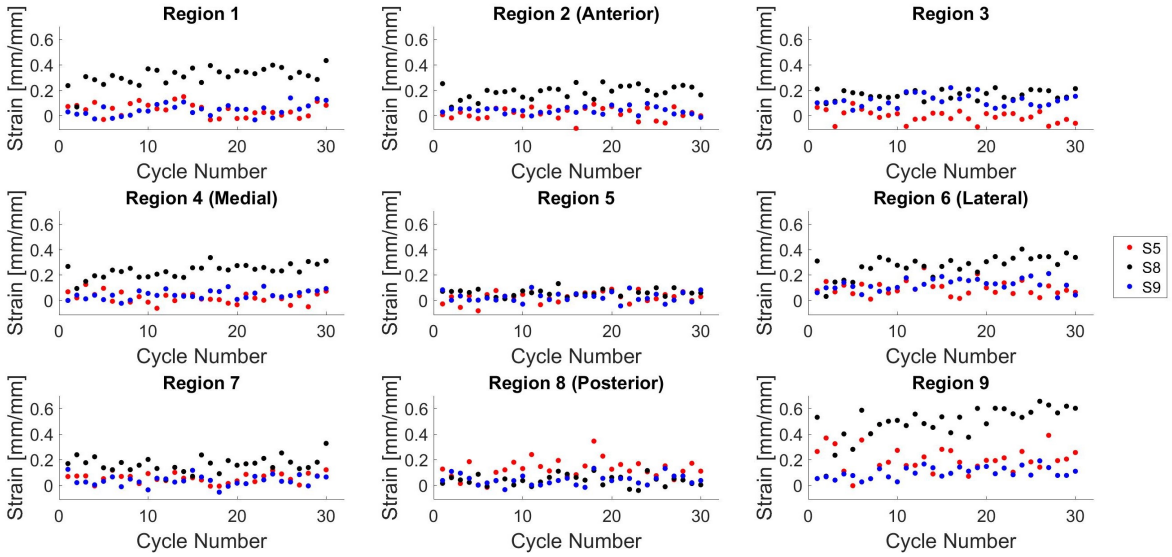

Figure 18: Changes in strain over cycles. Increasing trends can be seen in regions 1, 4, 6, and 9.

Strain

Surface strain of the superior capsule-tendon complex data was evaluated for each cycle. Nine regions of strain were quantified from the displacement grid (Figure 12, Table 5). Two of the three specimens showed a consistent peak strain magnitude and location (region 9, posterior-lateral corner of the capsule), however the third specimen did not show consistency in peak strain location. No regions showed decreasing strain, and the strain in most regions (2, 3, 5, and 8) was constant. One specimen showed larger increases in strain than the other two (Figure 18).

Strain values through the first seven cycles alone were also examined (Figure 19). The average strains in cycle 1 were larger (0.164 ± 0.095) than their cycle 7 counterparts (0.147 ± 0.080), however a paired t-test did not find the difference to be significant ($p = 0.175$).

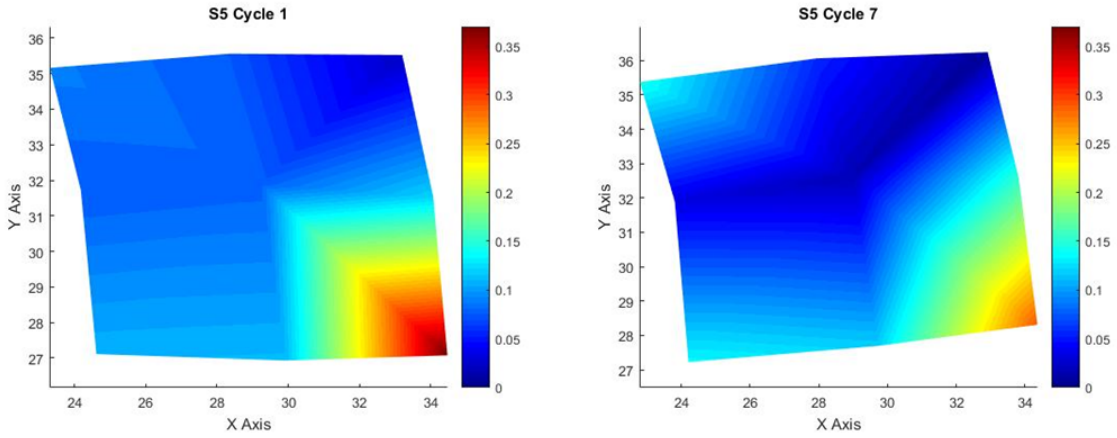

Figure 19: Strain for specimen S5 at the end of cycles 1 and 7, plotted on the same color scale. While there are some slight changes in peak strain and strain at certain locations, the strain distribution is largely unchanged.

Table 5: Average strain values by region for all specimens, shown across all cycles, cycles 1-6, and cycles 7-30.

Strain [mm/mm]

S5	R1	R2	R3	R4	R5	R6	R7	R8	R9	Overall
mean	0.05	0.02	-0.01	0.02	0.03	0.09	0.06	0.13	0.21	0.07
mean 1-6	0.05	-0.01	0.03	0.06	-0.01	0.10	0.06	0.06	0.24	0.07
mean 7-30	0.04	0.02	-0.02	0.01	0.04	0.09	0.05	0.14	0.20	0.07

S8	R1	R2	R3	R4	R5	R6	R7	R8	R9	Overall
mean	0.31	0.19	0.16	0.23	0.06	0.28	0.16	0.04	0.49	0.21
mean 1-6	0.24	0.15	0.16	0.19	0.07	0.18	0.18	0.03	0.35	0.17
mean 7-30	0.33	0.20	0.17	0.25	0.06	0.30	0.16	0.04	0.53	0.23

S9	R1	R2	R3	R4	R5	R6	R7	R8	R9	Overall
mean	0.05	0.04	0.12	0.05	0.03	0.12	0.04	0.04	0.10	0.06
mean 1-6	0.01	0.05	0.09	0.02	0.02	0.09	0.04	0.05	0.06	0.05
mean 7-30	0.05	0.04	0.12	0.05	0.03	0.13	0.03	0.04	0.11	0.07

2.4 Discussion

In this study, we aimed to develop a novel test methodology for investigating whether adduction torques contribute to damage of the Supraspinatus tendon and/or capsule. The strongest evidence that mechanical damage occurs due to repeated powered adduction is the Supraspinatus tension lost between cycles. However, the decay of this loss in tensile strength with increasing cycles suggests that the initial few exposures to sudden high-torque loading are initiating the bulk of damage to the tissue. There was no visible tissue damage, suggesting that damage is likely occurring in the form of micro-tears within the tendon-capsule complex. We believe that this damage is indicative of the failure of collagen fibers (and cross links [8]) that initially absorb the bulk of the load, after which

load is transferred to other collagen fibers upon re-tension. This is similar to the hypotheses derived from the fiber recruitment model [11], where fibers are "recruited" as the strain in the tendon increases.

As cycle number increased, the tendon clamp was displaced more to maintain the initial tension. It appears that the effect of doing this is to stretch out and effectively sharpen the toe region in collagen fiber recruitment, where we see a decrease in k_1 followed by a slight increase in k_2. In a living person, this would require the Supraspinatus muscle to contract/displace further to generate the same resulting motion of the arm.

From the data, a generalized model was created to attempt to explain the slack-stiffening patterns observed (Figure 16-A). When looking at a force-displacement diagram for an individual specimen and cycle (like in Figure 16-B), there are distinct changes in stiffness as the displacement increases. These changes are thought to be the recruitment of the tendon (region I in Figure 16), the straining of the tendon (region II), and the straining of the tendon and capsule together (region III). These patterns of stiffness changes were tracked and fit to the general model, which may be an indicator of the degree of microdamage in the tissue from the macroscopic properties. Specimens with stiffness patterns starting in region II are believed to have a greater degree of tissue damage when compared to those starting in region I.

The variability seen in the force-displacement curves between specimens is related to the tensile load during powered adduction, and suggests different degrees of existing damage in the specimens prior to testing. The specimens used in this study had a mean age of 55.8 years, and others have suggested that the 65.3% of all rotator cuff tears are asymptomatic [22].

The strain data did not show evidence of a decrease in mechanical resistance over cycles. There was no significant change in the maximum strains seen within a specimen throughout testing, although local strains in different regions did result in higher strains in the later cycles, particularly in the medial portion of the tendon-capsule complex. The lack of apparent change in the strain of the tendon-capsule complex (Figure 19) suggests that the capsule is not undergoing measurable damage during testing. This is in contrast to the tensile loss measured on the tendon alone as well as the decrease in k_3 stiffness (Figure 17). The results suggest that while the capsule plays a role in absorbing load, the damage during this motion is primarily concentrated in the tendon.

There are several limitations to this study. We could not quantify the initial anatomical state of the Supraspinatus tendon to determine the presence of preexisting tears. The estimation of Supraspinatus tension takes the geometry of the shoulder into account and combines this with experimentally mea-

sured results to estimate Supraspinatus pretension. This estimate relies on the findings from Sharkey et al. [30], and assumes relatively consistent muscle moment arms between subjects. More work is needed to determine the reliability of this estimate.

In the future, this study should be expanded by increasing the number of specimens tested, and analyzing the nature of collagen micro-tearing in the specimen with pre- and post-test imaging analysis. Load cells should be replaced with higher data acquisition rate models. Additionally, as the data sets of specimens increase, a damage model may be developed to more completely identify the rate at which damage occurs in the tendon.

2.5 Conclusion

We have demonstrated that there is a decay in the Supraspinatus tendon's ability to support load during sudden adduction motions. Rotator cuff tears may be fatigue-driven where repeated trauma gradually weakens the tissue prior to failure rather than the result of a blunt immediate trauma. However, the immediate decrease in load capacity suggests that the damage associated with decreased tendon strength occurs relatively early in the fatigue cycle. Our data suggests that preventative methods to protect the shoulder from fatiguing via a brace or other ergonomic considerations should be employed to mitigate this risk factor. Further work is needed to determine how shoulder biomechanical function in vivo is affected by repeated exposure to torques and to relate tissue microstructure to macroscopic tendon properties.

3 Future Work and Recommendations

Data produced in this study suggests several directions for subsequent work. For this study, one potential problem/limitation was the relatively low sampling frequency (62.5Hz) of the load cell used to measure Supraspinatus tension. The same equipment used could be set to 125Hz, but this would increase noise in the measurements. With the testing methodology and mechanism implemented and working, purchasing and using a higher quality load cell and DAQ that are capable of higher sampling rates is recommended. The improved data resolution would be particularly useful in capturing the peak load that the specimen sees during testing. In some specimens the peak load ratio (PLR: defined as the peak tension normalized to the initial tension) showed a promising decaying trend in most specimens, however there is doubt that the true peak load was captured given the relatively low sampling frequency, making this information less valuable as a metric for studying damage.

This study employed the use of a 100fps camera to track surface strain of the capsule and tendon with a 3 by 4 dot matrix. Local strain was computed through a series of MATLAB scripts developed for this purpose, and while the process is fairly streamlined there is a time-consuming manual element that introduces potential human error. To avoid these issues moving forward, there are two viable options: implementing digital image correlation (DIC) or writing an image processing script in MATLAB to find the centers of the dots in the dot matrix. Each method presents challenges: for the DIC, there is a considerable amount of shaking in the system which has at times lead to image blurring. Additionally, the speed of the test would likely necessitate the use of a higher frame-rate camera. For image processing code to track the dot centers, having a clean dot pattern (no smudges or bleeding, very circular) would be critical to avoid problems arising from image blurring. Possible fixes to the image blurring issue include upgrading the camera (higher frame rate) and software to process images in order to remove/minimize blurring. Upgrading the strain acquisition methodology could lead to a less tedious and time consuming manual process, and less susceptibility to error.

One of the biggest limitations this study faced was a lack of quantifiable information about the initial state of the tendons, particularly regarding the degree of microtearing in the tendon. During testing, there was considerable variability in the force response data, which I hypothesize was caused by varying levels of preexisting damage to the tendon microstructure. Unfortunately, without imaging assessments of the tissue microstructure this idea cannot be confirmed. This information would be very important in the development of a full damage model for Supraspinatus and would be highly valuable in relating the microscopic tendon properties to macroscopic performance and health of the tendon.

This study chose to focus on one initial angle and range of powered travel, however this does not necessarily need to be the case. The test apparatus was designed such that the initial angle of the scapula relative to the range of motion can be rotated (in plane) a full 360°, with 1° resolution. Additionally, the powered range of motion (relative to the scapula) can be varied between approximately 0° and 60°. This freedom and flexibility in the test apparatus means that this system can test other muscles, motions, and arm angles with powered impulse abduction and adduction arm rotations. Such freedoms allow for the exploration of other muscle and tendon force responses in similar loading conditions. It is also possible to replace the drill with a motor (and gearbox), which would allow for traditional cyclic fatigue tests under low-speed conditions.

References

[1] David C. Ackland, Ponnaren Pak, Martin Richardson, and Marcus G. Pandy. Moment arms of the muscles crossing the anatomical shoulder. *Journal of Anatomy*, 213(4):383–390, 2008.

[2] Anthony Cooper & Amjid Ali. Rotator cuff tears. *J Am Geriatr Soc*, 41(1):90, 1993.

[3] Dan Anton, Lee D. Shibley, Nathan B. Fethke, Jennifer Hess, Thomas M. Cook, and John Rosecrance. The effect of overhead drilling position on shoulder moment and electromyography. *Ergonomics*, 44(5):489–501, 2001.

[4] T Bunker. Rotator cuff disease. *Current Orthopaedics*, pages 223–233, 2002.

[5] M.D. Christopher R. Adams, M.D., Angelica M. DeMartino, M.S., George Rego, M.P.H., P.A.-C., Patrick J. Denard, M.D., and Stephen S. Burkhart. The Rotator Cuff and the Superior Capsule: Why We Need Both. *Arthroscopy: The Journal of Arthroscopic and Related Surgery*, 32(12):2628–2637, 2016.

[6] Alexis Chiang Colvin, Natalia Egorova, Alicia K Harrison, Alan Moskowitz, and Evan L Flatow. National trends in rotator cuff repair. *The Journal of bone and joint surgery. American volume*, 94(3):227–33, 2012.

[7] Makita Corporation. Cordless Drill Driver Instruction Manual XFD07Z.

[8] Baptiste Depalle, Zhao Qin, Sandra J. Shefelbine, and Markus J. Buehler. Influence of cross-link structure, density and mechanical properties in the mesoscale deformation mechanisms of collagen fibrils. *Journal of the Mechanical Behavior of Biomedical Materials*, 52:1–13, 2015.

[9] Anthony F. DePalma. Surgical anatomy of the rotator cuff and the natural history of degenerative periarthritis. Surg Clin North Am. 1963;43:1507-1520. *Clinical orthopaedics and related research*, 466(3):543–551, 2008.

[10] Glenn S. Fleisig, James R. Andrews, Charles J. Dillman, and Rafael F. Escamilla. Kinetics of Baseball Pitching with Implications About Injury Mechanisms. *The American Journal of Sports Medicine*, 23(2):233–239, 1995.

[11] Kristi A. Hansen, Jeffrey A. Weiss, and Jennifer K. Barton. Recruitment of Tendon Crimp With Applied Tensile Strain. *Journal of Biomechanical Engineering*, 124(1):72, 2002.

[12] Takashi Hashimoto, Katsuya Nobuhara, and Tetsuo Hamada. Pathologic Evidence of Degeneration as a Primary Cause of Rotator Cuff Tear. *Clinical Orthopaedics and Related Research*, 415(415):111–120, 2003.

[13] R.J. Hawkins and J.C. Kennedy. Impingement syndrome in athletes. *The American Journal of Sports Medicine*, 8(3):151–158, 1980. PMID: 7377445.

[14] Eiji Itoi, Lawrence J Berglund, John J Grabowski, Fredrick M Schultz, Eric S Growney, Bernard F Morrey, and Kai-Nan An. Tensile properties of the supraspinatus tendon. *Journal of Orthopaedic Research*, 13(4):578–584, 1995.

[15] Nitin B Jain, Laurence D Higgins, Elena Losina, Jamie Collins, Philip E Blazar, and Jeffrey N Katz. Epidemiology of musculoskeletal upper extremity ambulatory surgery in the United States. *BMC Musculoskeletal Disorders*, 15(1):4, 2014.

[16] Ulf Järvholm, Gunnar Palmerud, Peter Herberts, Christian Högfors, and Roland Kadefors. Intramuscular Pressure and Electromyograhy in the Supraspinatus Muscle at Shoulder Abduction.pdf. *Clinical Orthopaedics and Related Research*, 245:102–109, 1989.

[17] M Katayose and D J Magee. The cross-sectional area of supraspinatus as measured by diagnostic ultrasound. *The Journal of bone and joint surgery. British volume*, 83(May):565–568, 2001.

[18] Higgins L.D., Von Keudell A., and Jain N. Cost-effectiveness of rotator cuff repair. *Arthroscopy - Journal of Arthroscopic and Related Surgery*, 29(6 SUPPL. 1):e14, 2013.

[19] Patrick J. McMahon, Richard E. Debski, William O. Thompson, Jon J P Warner, Freddie H. Fu, and Savio L Y Woo. Shoulder muscle forces and tendon excursions during glenohumeral abduction in the scapular plane. *Journal of Shoulder and Elbow Surgery*, 4(3):199–208, 1995.

[20] Lori A Michener, Philip W McClure, and Andrew R Karduna. Anatomical and biomechanical mechanisms of subacromial impingement syndrome. *Clinical biomechanics*, 18(5):369–379, 2003.

[21] R. Matthew Miller, Yoshimasa Fujimaki, Daisuke Araki, Volker Musahl, and Richard E. Debski. Strain distribution due to propagation of tears in the anterior supraspinatus tendon. *Journal of Orthopaedic Research*, 32(10):1283–1289, 2014.

[22] Hiroshi Minagawa, Nobuyuki Yamamoto, Hidekazu Abe, Masashi Fukuda, Nobutoshi Seki, Kazuma Kikuchi, Hiroaki Kijima, and Eiji Itoi. Prevalence of symptomatic and asymptomatic rotator cuff tears in the general population: From mass-screening in one village. *Journal of Orthopaedics*, 10(1):8–12, 2013.

[23] Vangsness CT Jr. Narvy SJ, Ahluwahlia A. Analysis of Direct Costs of Outpatient Arthroscopic Rotator Cuff Repair. *American Journal of Orthopedics*, 45(January):E7–11, 2016.

[24] Andrew Neviaser, Nelly Andarawis-Puri, and Evan Flatow. Basic mechanisms of tendon fatigue damage. *Journal of Shoulder and Elbow Surgery*, 21(2):158–163, 2012.

[25] Samuel J. Olsen, Glenn S. Fleisig, Shouchen Dun, Jeremy Loftice, and James R. Andrews. Risk Factors for Shoulder and Elbow Injuries in Adolescent Baseball Pitchers. *The American Journal of Sports Medicine*, 34(6):905–912, 2006.

[26] Jennifer M. Ortman, Victoria a. Velkoff, and Howard Hogan. An aging nation: The older population in the United States. *Economics and Statistics Administration, US Department of Commerce*, 1964:1–28, 2014.

[27] Hafizur Rahman, Eric Currier, Marshall Johnson, Rick Goding, Amy J. Wagoner Johnson, and Mariana Kersh. Primary and secondary consequences of rotator cuff injury on joint stabilizing tissues in the shoulder. *Journal of Biomechanical Engineering*, 139(November):1–10, 2017.

[28] P. Reilly, I. Macleod, R. Macfarlane, J. Windley, and R. J H Emery. Dead men and radiologists don't lie: A review of cadaveric and radiological studies of rotator cuff tear prevalence. *Annals of the Royal College of Surgeons of England*, 88(2):116–121, 2006.

[29] Shane T. Seroyer, Shane J. Nho, Bernard R. Bach, Charles A. Bush-Joseph, Gregory P. Nicholson, and Anthony A. Romeo. The kinetic chain in overhand pitching: Its potential role for performance enhancement and injury prevention. *Sports Health*, 2(2):135–146, 2010.

[30] Neil A. Sharkey, Richard A. Marder, and Peter B. Hanson. The entire rotator cuff contributes to elevation of the arm. *Journal of Orthopaedic Research*, 12(5):699–708, 1994.

[31] Neil A. Sharkey, Tait S. Smith, and David C. Lundmark. Freeze clamping musculo-tendinous junctions for in vitro simulation of joint mechanics. *Journal of Biomechanics*, 28(5):631–635, 1995.

[32] DuFang Shi, DongMei Wang, ChengTao Wang, and Anmin Liu. A novel, inexpensive and easy to use tendon clamp for in vitro biomechanical testing. *Medical Engineering and Physics*, 34(4):516–520, 2012.

[33] Robert Z. Tashjian. Epidemiology, Natural History, and Indications for Treatment of Rotator Cuff Tears. *Clinics in Sports Medicine*, 31(4):589–604, 2012.

[34] Siegbert Tempelhof, Stefan Rupp, and Romain Seil. Age-related prevalence of rotator cuff tears in asymptomatic shoulders. *Journal of Shoulder and Elbow Surgery*, 8(4):296–299, 1999.

[35] Glenn C. Terry and Thomas M. Chopp. Functional Anatomy of the Shoulder. *Journal of Athletic Training*, 35(3):248–255, 2000.

[36] Michael J. Tuite, John R. Turnbull, and John F. Orwin. Anterior versus posterior, and rim-rent rotator cuff tears: Prevalence and MR sensitivity. *Skeletal Radiology*, 27(5):237–243, 1998.

[37] G. Walch, P. Boileau, E. Noel, and S. T. Donell. Impingement of the deep surface of the supraspinatus tendon on the posterosuperior glenoid rim: An arthroscopic study. *Journal of Shoulder and Elbow Surgery*, 1(5):238–245, 1992.

[38] Daniëlle A W M Van Der Windt, Elaine Thomas, Daniel P Pope, Andrea F De Winter, Gary J Macfarlane, Lex M Bouter, and Alan J Silman. Occupational risk factors for shoulder pain : a systematic review. pages 433–442, 2000.

[39] David A. Winter. *Biomechanics and Motor Control of Human Movement, 4th Edition.* Wiley, 2009.

[40] Wen Wu, Peter V S Lee, Adam L. Bryant, Mary Galea, and David C. Ackland. Subject-specific musculoskeletal modeling in the evaluation of shoulder muscle and joint function. *Journal of Biomechanics*, 49(15):3626–3634, 2016.

[41] Ken Yamaguchi, A. Marc Tetro, Oren Blam, Bradley A. Evanoff, Sharlene A. Teefey, and William D. Middleton. Natural history of asymptomatic rotator cuff tears: A longitudinal analysis of asymptomatic tears detected sonographically. *Journal of Shoulder and Elbow Surgery*, 10(3):199–203, 2001.

Appendix A Peak Load Ratio

One of the metrics calculated but not used was the deterioration of the peak load sustained during each cycle, which we normalized to the starting load for each cycle and plotted as a function of cycles for each specimen. The Peak Load Ratio (PLR) did not show a single common trend across all specimens, although specimens did show decreasing trends by the latter portion of cycles (Figure 20).

The PLR data might indicate the degree of pre-existing damage in specimens: specimen S5 demonstrates little capacity to resist additional load and did not show up until region II in our generalized stiffness model. Conversely, specimen S8 showed initially large and subsequent decay in PLR and shows up in region I of the generalized stiffness model—both indicators of an initially healthy tissue. Information regarding the degree of micro-tearing already present in the cadavers could potentially address the differences seen in the PLR data, however without this additional information it is difficult to find meaning in the results. Also limiting the PLR data was the relatively low sampling rate available, which likely allowed for the true peak load to be missed in some cycles.

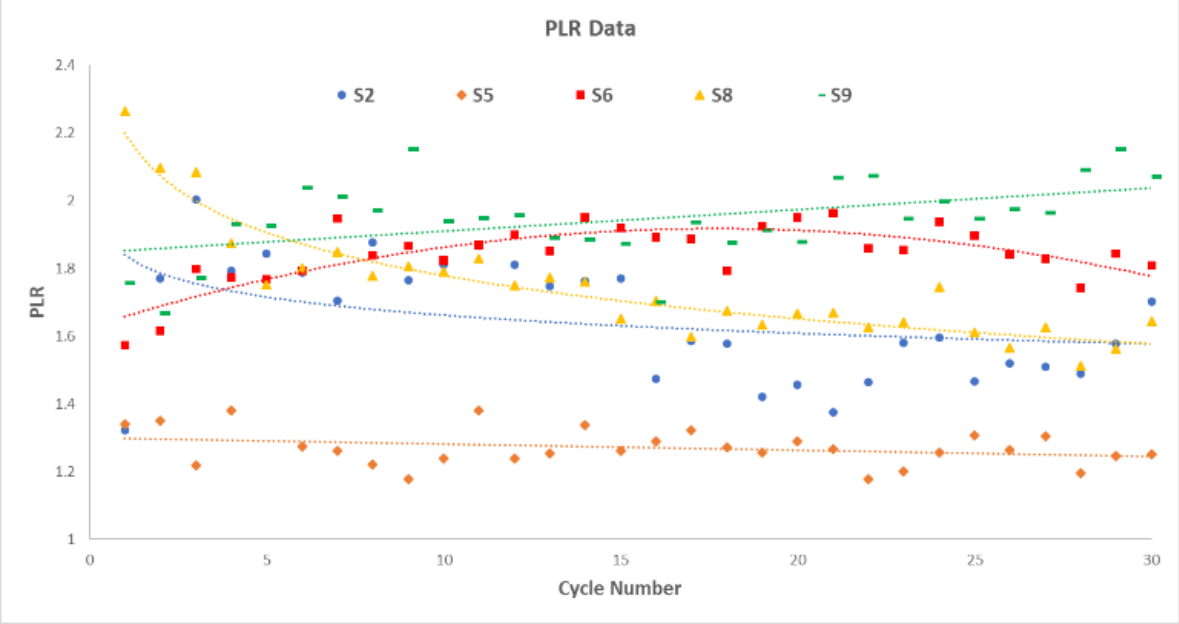

Figure 20: Peak Load Ratio (PLR) data with best fits shown. The general trends show decreasing ability to bear load in the latter stages for most specimens, although not in all cases.